Biosensors and Bioelectronics 66 (2015) 208–215

Contents lists available at ScienceDirect

Biosensors and Bioelectronics

journal homepage: www.elsevier.com/locate/bios

Evaluation of a carbon nanotube-titanate nanotube nanocomposite as an electrochemical biosensor scaffold

Xiaoqiang Liu [a,*], Rui Yan [a], Jiamei Zhang [a], Jie Zhu [a], Danny K.Y. Wong [b,*]

[a] Institute of Environmental and Analytical Sciences, College of Chemistry and Chemical Engineering, Henan University, Kaifeng, Henan Province 475004, PR China

[b] Department of Chemistry and Biomolecular Sciences, Macquarie University, Sydney, NSW 2109, Australia

ARTICLE INFO

Article history:
Received 18 August 2014
Received in revised form
14 November 2014
Accepted 17 November 2014
Available online 20 November 2014

Keywords:
MWCNT–TNT nanocomposites
Electrochemical biosensor
Immobilisation materials
Direct electrochemistry
Catalytic capability

ABSTRACT

A significant aspect of this work is the development of a multi-wall carbon nanotube (MWCNT)-titanate nanotube (TNT) nanocomposite to serve as a biocompatible scaffold with high conductivity on a biosensor surface. Unlike other scaffolds consisting of MWCNTs alone or TNTs alone, the MWCNT–TNT nanocomposite synergistically provides excellent biocompatibility, good electrical conductivity, low electrochemical interferences and a high signal-to-noise ratio. For comparison, after characterising a scaffold consisting of MWCNTs alone, TNTs alone and a MWCNT–TNT nanocomposite using several spectroscopic techniques, the analytical performance of a horseradish peroxidase (HRP) electrochemical biosensor was evaluated using cyclic voltammetry and differential pulse voltammetry. The scaffold consisting of MWCNTs alone displayed a high background charging current, a low signal-to-noise ratio and distinct electrochemical interference from its surface functional groups. In contrast, the direct electrochemistry and the catalytic capability of HRP at MWCNT–TNT modified biosensors towards H_2O_2 was demonstrated to be ~51% and ~144% enhanced, respectively, compared to those at TNT modified biosensors. Meanwhile, MWCNT–TNT nanocomposite modified HRP biosensors also exhibited higher sensitivity (4.42 μA mM^{-1}) than TNT modified HRP biosensors (1.48 μA mM^{-1}). The above superior performance was attributed to the improved properties of MWCNT–TNT nanocomposite as biosensor scaffold compared to its two individual components by complementing each component and synergistically sustaining the characteristic features of each component.

1. Introduction

In recent years, various nano-materials have been designed and applied as immobilisation materials to electrochemical biosensors due to their unique features including the ability to promote the direct electron transfer between a targeted biomolecule and the electrode surface (Holland et al., 2011; Pumera et al., 2007; Qureshi et al., 2009; Si et al., 2011). These nanomaterials will generally also exhibit high electrical conductivity, large surface area, biocompatibility and chemical stability, etc. Evidently, a single nanomaterial is unlikely to simultaneously offer several, if not all, of these beneficial features. This has led to recent developments and applications of composite nano-materials capable of synergistically contributing the advantages of their individual components and thereby significantly reducing their shortcomings. For example, carbon nanotubes (CNTs) have attracted great interest in electrochemistry owing to their characteristic properties including electrical conductivity, surface area, electric-capacitance, mechanical and chemical stability (Coleman et al., 2006). For example, by incorporating horseradish peroxidase (HRP) in a multi-wall carbon nanotubes-chitosan film on a biosensor, direct electrochemistry and electrocatalysis of HRP achieved at this biosensor aided in yielding a 16.7–740 μM linear range and a 10.3 μM detection limit (Qian and Yang, 2006). However, similar to other carbon materials, CNTs often display undesirably high charging currents arising from their super conductivity and electrochemical interferences caused by oxygen-containing groups on their surface, resulting in low signal-to-noise ratios (Qian and Yang, 2006; Serafín et al., 2013). Hence, complementary materials that will improve on their biocompatibility and decrease the charging current are rigorously being sought.

In addition to CNTs, TiO_2 or titanate (i.e. $Na_2Ti_2O_4(OH)_2$) nanomaterials including nanoparticles (Wang et al., 2010), nanobelts (Wang et al., 2009b), nanowires (Lin et al., 2003) and nanorods

* Corresponding authors.
E-mail addresses: xq_liu1975@yahoo.com (X. Liu), Danny.Wong@mq.edu.au (D.K.Y. Wong).

http://dx.doi.org/10.1016/j.bios.2014.11.028
0956-5663/

(Joo et al., 2005) have been synthesised and increasingly applied to photochemistry and electrochemistry due to their biocompatibility, high porosity, and anti-oxidising properties (Si et al., 2011; Zhang et al., 2011). For example, a H_2O_2 electrochemical biosensor based on HRP immobilised on a Au-modified TiO_2 nanotube composite exhibited a wide linear range (5–400 μM), a low detection limit (2 μM) and high stability (95% of initial current response retained after 21 days) (Kafi et al., 2008). Despite the advantages of TiO_2 or titanate nano-materials highlighted above, their electrical conductivity has been compromised because of their semi-conducting properties. Clearly, composites of TiO_2 or titanate nanomaterials and CNTs will complement the shortcomings of the individual components while retaining their merits.

Although nanocomposites consisting of CNT and TiO_2 nanomaterials have also been prepared and used in photocatalysis and photovoltaic devices in recent years (Chen et al., 2011; Muduli et al., 2009; Wang et al., 2009a), there have been limited applications to the construction of electrochemical biosensors. In 2009, Pang et al. (Pang et al., 2009) have fabricated a glucose biosensor based on a Pt nanoparticle-decorated CNT|TiO_2 nanotube array composite, which was prepared by electrochemically oxidising a titanium foil, followed by chemical vapour deposition of CNTs in the inner wall of the TiO_2 nanotube array formed. While these TiO_2 nanotube arrays are more conducting than titanate nanotubes (TNTs), their non-porous structures make them difficult to be used as an immobilisation matrix for biomolecules. The present work aims at evaluating the feasibility of using multi-wall CNT (MWCNT)-titanate composites as electrode materials. Herein, TNTs were applied in conjunction with MWCNTs because TNTs have a high specific surface area, similar dimensions to many biomolecules (e.g. HRP and glucose oxidase). In this way, they will provide a larger interfacial contact area with biomolecules than TiO_2 nanoparticles to accommodate a higher load of biomolecules (Perera et al., 2012). In addition, the high specific surface area, excellent biocompatibility and abundant surface functional groups of TNTs will increase the load of redox enzymes and contribute to sustaining their bioactivity.

In this work, TiO_2 nanoparticles were hydrothermally grown into TNTs, which were then incorporated with MWCNTs in a Teflon-lined autoclave. Three designs of HRP electrochemical biosensors were developed using a MWCNT–TNT nanocomposite, MWCNTs alone and TNTs alone as electrode immobilisation materials, respectively, for comparison purpose. Nafion and the room temperature ionic liquid, brominated 1-decyl-3-methyl imidazole ([Demim]Br), were also used as anchoring agents to immobilise the MWCNT–TNT nanocomposite|[Demim]Br|Nafion scaffold on the biosensor surface. Finally, electrochemical behaviour and analytical performance of these biosensors was studied using cyclic voltammetry and differential pulse voltammetry to determine the optimal electrode immobilisation material for the HRP biosensors.

2. Experimental

2.1. Reagents and instruments

Short chain carboxylic acid functionalised (3.86% weight/weight) MWCNTs (30–50 nm outside diameter, 0.5–2 μm length) were purchased from Chengdu Organic Chemical Co., Ltd., Chinese Academy of Sciences, China. TiO_2 nanoparticles were acquired from Tianjin Chemical Reagent Co. Ltd., China. HRP, Nafion and [Demim]Br were purchased from Sigma-Aldrich. Phosphate buffered saline (PBS, 0.1 M) containing 50 mM Na_2HPO_4, 50 mM KH_2PO_4 and 100 mM KCl was adjusted to pH 7.2 by adding 0.1 M NaOH. All solutions were prepared using Milli-Q purified water.

Electrochemical measurements were performed using a CHI630C electrochemical workstation (CH Instruments, Shanghai, China). A conventional three-electrode system, consisting of a glassy carbon (3 mm in diameter) working electrode, a platinum wire counter electrode and a Ag|AgCl (3.0 M KCl) reference electrode, was used. All electrodes were purchased from Gaoshiruilian Co. Ltd., Wuhan, China. Electrochemical impedance spectroscopy was conducted using an IM6ex electrochemical workstation (Zahner, Germany). The chemical composition and morphology of nanocomposites were characterised by transmission electron microscopy (TEM; Tecnai G2 20 transmission electron microscope USA), X-ray diffraction (XRD; Bruker D8 Advance X-ray diffraction spectrometer, Germany) with a Cu Kα radiation ($\lambda = 1.5406$ nm), and Fourier transform infra-red spectrometry (FTIR; Nicolet 170 Fourier transform infra-red spectrometer, USA).

2.2. Preparation of MWCNT–TNT composites

In the synthesis of a MWCNT–TNT composite, 10 mg MWCNTs was initially added to 1 mL of 1 M sodium dodecyl sulfate solution. Next, 19 mL doubly distilled water was added and the mixture was ultrasonicated for 1 h. Following that, 500 mg TiO_2 nanoparticles was added to a continuously stirred MWCNT dispersion. Then, 20 mL of 20 M NaOH aqueous solution was added and the mixture was transferred to a Teflon-lined autoclave, followed by hydrothermal reaction at 120 °C for 30 h. A grey product obtained was washed with Milli-Q water 3 times, then adjusted with 0.1 M HCl to pH 7, washed with Milli-Q water 3 times again, followed by centrifugation. Finally, the product was dried at 80 °C for 5 h and then ground to powder. TNTs alone were prepared by a similar process but without adding any MWCNTs.

2.3. Preparation of the HRP modified electrodes

The glassy carbon electrode (GCE) was sequentially polished in a slurry of 1 and 0.3 μm alumina powder, followed by sonication in Milli-Q water for 2–3 min, and then dried at room temperature. A mixture of HRP, MWCNT–TNT, [Demim]Br and Nafion was agitated at 4 °C for 4 h in a full temperature oscillation incubator before being applied to an electrode surface. In brief, 50 μL Nafion and 300 μL HRP aqueous solution (2 mg mL^{-1}) were mixed with the MWCNT–TNT composite and [Demim]Br (1:5, weight/weight). Finally, 4 μL of the mixture was applied to the GCE and dried at 4 °C. This electrode will thereafter be denoted as MWCNT–TNT|[Demim]Br|Nafion|HRP|GCE. For comparison, a TNT|[Demim]Br|Nafion|HRP|GCE and a MWCNT|[Demim]Br|Nafion|HRP|GCE were also fabricated using the same procedure.

2.4. Electrochemical measurements

All electrolytes were deoxygenated by high purity nitrogen for 15 min prior to the experiments and maintained under a nitrogen atmosphere during the experiments. Electrochemical impedance spectroscopic measurements were conducted in the presence of 5.0 mM $K_3[Fe(CN)_6]$ in 0.1 M KCl supporting electrolyte by applying an AC voltage of 4 mV amplitude in a frequency range from 100 kHz to 20 mHz under open circuit potential conditions. All results obtained were presented as Nyquist plots. In these experiments, all simulated Nyquist plots were obtained using an IM6ex AC impedance simulation and fitting programme.

3. Results and discussion

3.1. Optimisation of MWCNT–TNT nanocomposites

In this work, we have adopted a previously reported procedure (Yang et al., 2003) in which TiO_2 nanoparticles were hydrothermally reacted with concentrated NaOH to form TNTs. The flocculent and porous features of TNTs produced this way will facilitate the accommodation of a high load of biomolecules and will likely to offer better biocompatibility (Liu et al., 2013; Si et al., 2011). Their strong affinity to substrates and tubular geometry contribute to the ease of their immobilisation on different electrode surfaces. In addition, the abundant hydroxyl groups on the TNTs would aid in conjugating biomolecules or other nanomateirals to TNTs.

In preparing the MWCNT–TNT nanocomposites, we used cyclic voltammetry of 50 mM N_2-saturated PBS at a MWCNT–TNT nanocomposite modified electrode to optimise the MWCNT to TiO_2 nanoparticle mass ratio and the results are shown in Fig. 1. As discussed below, a cyclic voltammogram with a large charging current and also interfering signals was often obtained at a MWCNT (alone) modified electrode. Therefore, we have kept in this work the mass of MWCNTs constant at 10 mg and increased TiO_2 nanoparticles from 100 mg to 700 mg at an interval of 200 mg. Trace a in Fig. 1 shows the cyclic voltammogram obtained at a modified electrode in which 100 mg TiO_2 nanoparticles was used. Here, the redox peaks at -0.054 and -0.14 V were resulted from interfering signals of the surface oxygen-containing groups of MWCNTs and a substantial charging current are clearly visible in this voltammogram. However, as displayed in trace b, when 300 mg of TiO_2 nanoparticles was used, both the interfering signals and charging current have decreased by 166% and 140%, respectively. Eventually, when the mass of TNTs was further increased to 500 mg to obtain trace c, the interfering signals are no longer visible and the charging current has diminished to a comparable level to that at a naked glassy carbon electrode. However, when 700 mg of TiO_2 nanoparticles was used, white TiO_2 was observed in the hydrothermal reaction vessel in addition to the grey nanocomposites, indicating the presence of unreacted TiO_2 nanoparticles. These unreacted TiO_2 would decrease the electrical conductivity of nanocomposites.

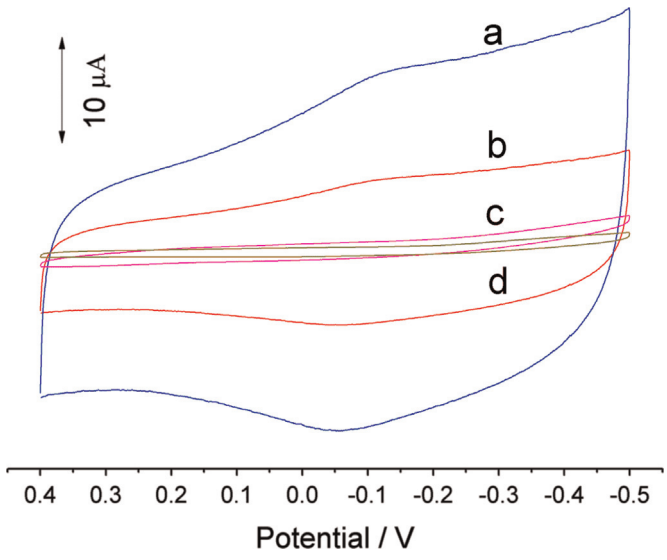

Fig. 1. Cyclic voltammograms of 50 mM N_2-saturated PBS (pH 7.2) at a MWCNT–TNT|[Demim]Br|Nafion|GCE fabricated using MWCNT to TiO_2 nanoparticle mass ratio of (a) 10 mg:100 mg; (b) 10 mg:300 mg; (c) 10 mg:500 mg; (d) 10 mg:700 mg; potential scan rate: 50 mV s^{-1}.

3.2. TEM, XRD, FT-IR characterisation of nanomaterials

Initially, the morphology of synthesised TNTs and MWCNT–TNT nanocomposites was characterised by TEM and the results are shown in Fig. 2(A) and (B), respectively. In Fig. 2(A), TNTs display a relatively uniform geometrical dimension with a diameter of approximately 10 nm and a length of a few hundreds nm. TNTs with such a small dimension provide a more biocompatible microenvironment for entrapped enzymes than other bulky TiO_2 nanomaterials such as TiO_2 nanoparticles and TiO_2 nanobundles (Liu et al., 2012; Wang et al., 2010). In Fig. 2(B), the longer (>1 μm) and curvy tubular structures with larger diameters (30–50 nm) correspond to MWCNTs, while the shorter tubes with a visibly smaller diameter ($\sim$10 nm) are TNTs. Notably, TNTs and MWCNTs are well intertwined with each other and some TNTs have grown on the outer surface of the MWCNTs. Clearly, it is challenging to produce a homogeneous mixture of two different tubular nanomaterials by simply mechanically agitating them. In our work, we have avoided this problem by hydrothermally growing TiO_2 nanoparticles into TNTs after mixing them with MWCNTs.

Next, XRD was used to characterise the crystal structure of TNTs, MWCNTs, and the MWCNT–TNT nanocomposites. Fig. 3 (A) shows the XRD pattern of TNTs (trace a), MWCNTs (trace b) and MWCNT–TNT nanocomposites (trace c). The diffraction peak of 9.6° in trace a and trace c is a notable feature of the tubular structure of TiO_2 nanomaterials (Zhang et al., 2004). In addition, the diffraction peaks of approximately 9.6°, 24.3°, 28.4° and 48.3° can be assigned to the (200), (110), (600) and (020) crystal faces of orthorhombic titanate nanotubes, which also supported the formation of TNT nanotubes (Pizem et al., 2002; Suzuki and Yoshikawa, 2004). In trace b, the intense 2θ peaks centred at 26.0° and 42.8° correspond to the (002) and (100) reflections of the graphite from MWCNTs (Wang and Zhou, 2011). It is noteworthy that the characteristic peaks of the MWCNTs (trace b) at 26.0° can also be observed clearly in the patterns of MWCNT–TNT composites (trace c), which provides another supporting indication of successful production of nanocomposite.

The FT-IR spectra of (a) TNTs alone, (b) MWCNTs alone and (c) MWCNT–TNT nanocomposites are shown in Fig. 3(B). In all three traces, the absorption peaks at 3426 cm^{-1} are induced by stretching vibration of the surface –OH group and the absorption peaks of 1628 cm^{-1} can be ascribed to bending vibration of the adsorbed H_2O molecules (Wang et al., 2009a). In trace a, TNTs displayed adsorption bands at 400–700 cm^{-1}, which are attributed to Ti–O stretching and Ti–O–Ti bridging (Chen et al., 2011). In trace c, the peak at $\sim$500 cm^{-1} is more intense than the corresponding peak in trace a. As reported previously, this absorption peak can be attributed to the combination of Ti–O–Ti and Ti–O–C vibration, demonstrating that chemical bonds were formed between MWCNTs and TNTs (Iwabuchi et al., 2004). Trace b shows the FT-IR spectrum of MWCNTs, where the peak at $\sim$1639 cm^{-1} is assigned to the bending vibration of the adsorbed H_2O molecules, 1389 cm^{-1} belongs to the C–OH stretching band and 1116 cm^{-1} belongs to the C–O stretches (Muduli et al., 2009), indicating the presence of oxygen-containing functional groups on its surface. These functional groups will aid in forming a nanocomposite between the MWCNTs and TNTs via hydrogen bonding, intermolecular forces or covalent binding.

3.3. Electrochemical impedance spectroscopic characterisation of nanomaterials

Electrochemical impedance spectroscopy is an effective technique for probing the interfacial properties of modified electrodes. In an imaginary impedance (Z_{Im}) *versus* real impedance (Z_{Re}) Nyquist plot, a semicircular feature in the high frequency region

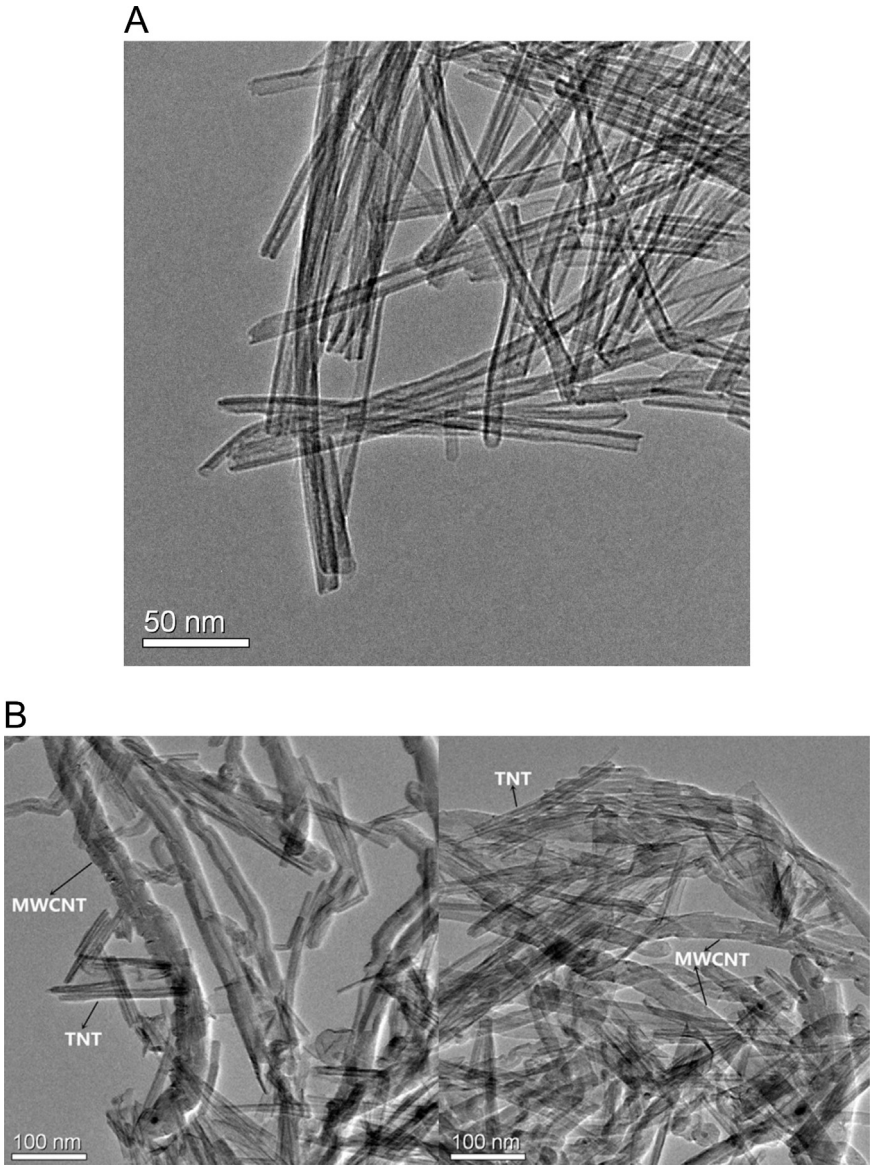

Fig. 2. TEM of (A) TNTs; (B) a MWCNT–TNT. nanocomposite.

arises from an electron transfer limited process, whereas the linear feature in the low frequency region is indicative of a diffusion-controlled process. The semicircle diameter corresponds to the electron-transfer resistance (R_{et}), which can be used to evaluate the electrical conductivity of the modified electrodes. As shown in Fig. 3(C), the MWCNT|GCE (trace a) and the MWCNT–TNT|GCE (trace b) displayed almost straight lines with an insignificant semicircle, indicating a nearly complete diffusion-control process and an excellent electrical conductivity. Based on an equivalent circuit (depicted in Fig. 3(C)) consisting of a constant phase element (C_{dl}), a R_{et} and a Warburg diffusion impedance (Z_W) in a parallel arrangement, which is then in series with a solution resistance (R_S), computer simulation was conducted to estimate the semicircle diameter in the high frequency region. As expected, the Nyquist plot obtained at the bare electrode (trace c) exhibits in the high frequency region a semicircle diameter of 530 Ω, compared to 1180 Ω in the Nyquist plot obtained at the TNT modified electrode (trace d), demonstrating a higher resistance of TNT|GCE than that of a bare GCE, the MWCNT|GCE and the MWCNT–TNT|GCE.

3.4. Electrochemical characterisation of HRP modified electrodes

Fig. 4(A) shows the cyclic voltammograms of a N_2-saturated pH 7.2 PBS at (a) MWCNT|[Demim]Br|Nafion|GCE and (b) MWCNT|[Demim]Br|Nafion|HRP|GCE at a scan rate of 50 mV s^{-1}. Here, the charging currents at both MWCNT|[Demim]Br|Nafion (trace a) and MWCNT|[Demim]Br|Nafion|HRP modified electrodes (trace b) exceeded 100 μA, which may prohibit achieving a good signal-to-noise ratio at the modified electrodes. The cyclic voltammogram obtained at the MWCNT|[Demim]Br|Nafion|GCE clearly exhibited two redox peaks at −0.24 V and 0.14 V, attributable to the oxygen-containing functional groups on a MWCNT surface (Chen et al., 2011). A corresponding pair of redox peaks with a larger peak current appeared in the cyclic voltammograms obtained at MWCNT|[Demim]Br|Nafion|HRP|GCE. These redox peaks may be ascribed to both electrochemical interferences from MWCNT surface groups and the direct electrochemistry of HRP (Liu et al., 2013). Therefore, MWCNTs alone are not an appropriate electrode immobilisation material for enzyme biosensors.

The electrochemical performance of both MWCNTs–TNTs and TNTs as electrode immobilisation materials was evaluated and the

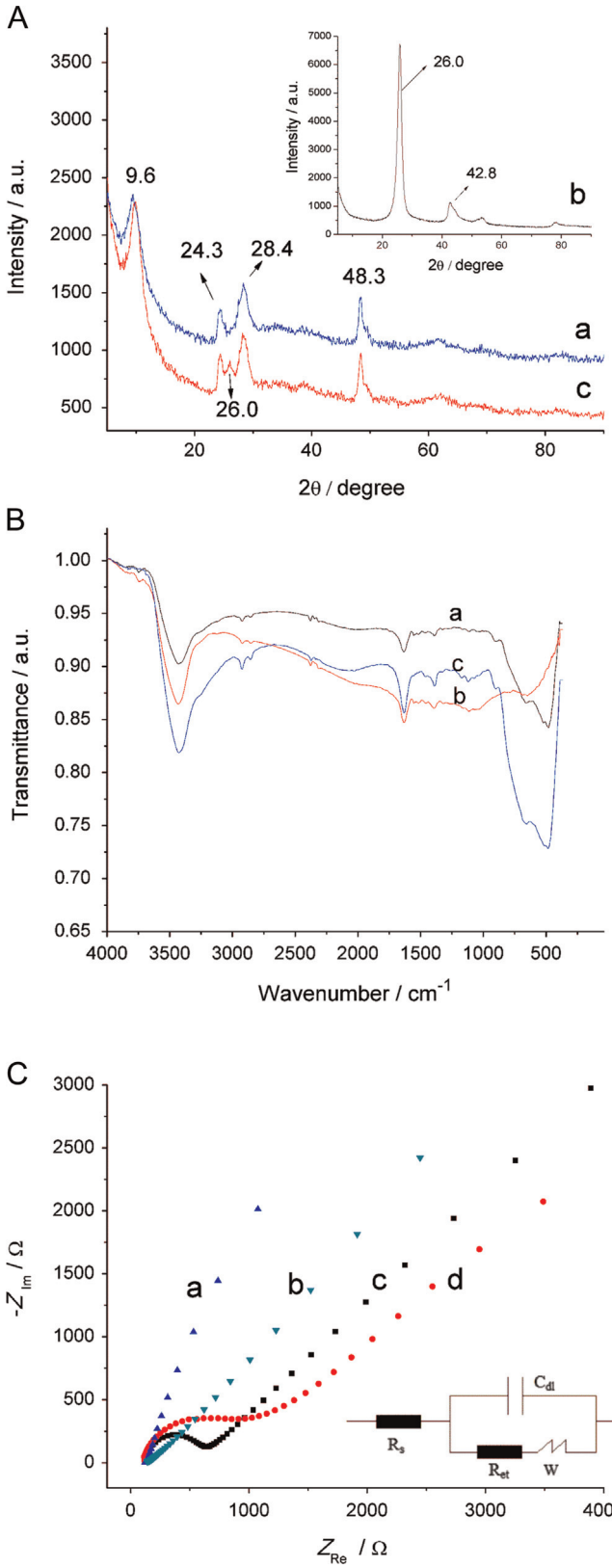

Fig. 3. (A) XRD pattern of (a) TNTs, (b) MWCNTs. and (c) a MWCNT–TNT. nanocomposite; (B) FT-IR spectra of (a) TNTs, (b) MWCNTs, and (c) a MWCNT–TNT. nanocomposite; (C) Nyquist plots of 5.0 mM $K_3[Fe(CN)_6]$ in 0.1 M KCl supporting electrolyte at (a) a MWCNT|GCE, (b) a MWCNT–TNT.|GCE, (c) a GCE, (d) TNT|GCE. Frequency ranges from 100 kHz to 20 mHz.

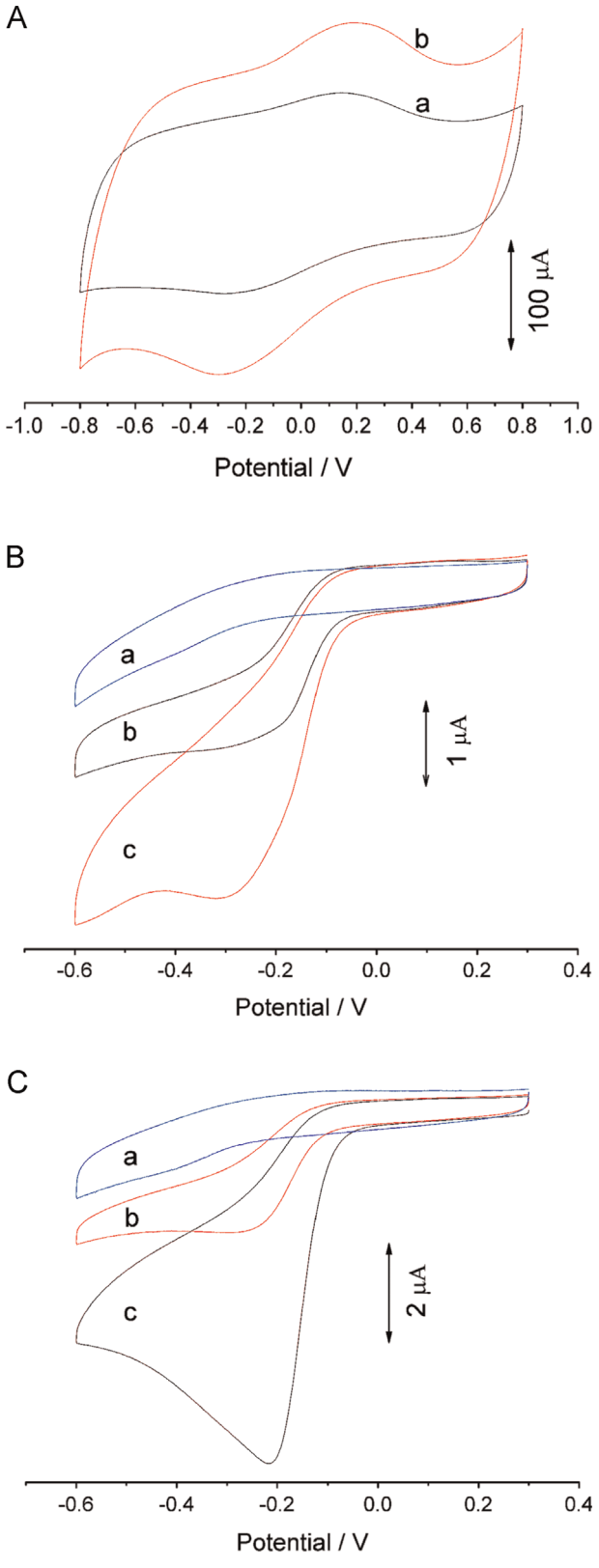

Fig. 4. (A) Cyclic voltammograms of 50 mM N_2-saturated PBS (pH 7.2) at (a) a MWCNT|[Demim]Br|Nafion|GCE and (b) a MWCNT|[Demim]Br|Nafion|HRP|GCE at a scan of 50 mV s^{-1}; (B) Cyclic voltammograms at (a) a TNT|[Demim]Br|Nafion|GCE, (b) a TNT|[Demim]Br|Nafion|HRP|GCE in the absence of 1.0 mM H_2O_2 in 50 mM N_2-saturated PBS (pH 7.2), and (c) in the presence of 1.0 mM H_2O_2 in 50 mM N_2-saturated PBS (pH 7.2). Scan rate: 50 mV s^{-1}; and (C) Cyclic voltammograms obtained at a MWCNT–TNT.|[Demim]Br|Nafion|GCE (trace a), MWCNT–TNT.|[Demim]Br|Nafion|HRP|GCE in the absence (trace b) and presence (trace c) of 1.0 mM H_2O_2 in 50 mM N_2-saturated PBS (pH 7.2) at a scan rate of 50 mV s^{-1}.

results are shown in Fig. 4(B) and (C), respectively. Fig. 4(B) shows the cyclic voltammograms at a TNT|[Demim]Br|Nafion|GCE (trace a) and a TNT|[Demim]Br|Nafion|HRP|GCE in the absence (trace b) and presence (trace c) of 1.0 mM H_2O_2, while Fig. 4(C) displays the cyclic voltammograms obtained at a MWCNT–TNT|[Demim]Br|Nafion|GCE (trace a) and MWCNT–TNT|[Demim]Br|Nafion|HRP|GCE in the absence (trace b) and the presence (trace c) of 1.0 mM H_2O_2. As displayed in trace a of Fig. 4(B) and (C), both TNT|[Demim]Br|Nafion|GCE and MWCNT–TNT|[Demim]Br|Nafion|GCE did not exhibit any visible redox peaks, supporting the feasibility of using TNTs and MWCNT–TNT nanocomposite as electrode immobilisation materials. In the absence of H_2O_2, the reduction current of HRP at the MWCNT-TNT modified electrodes (trace b, Fig. 4(C)) has increased by ~51% compared to that at the TNT modified electrodes (trace b, Fig. 4(B)). Also, the catalytic reduction current at the MWCNT–TNT|[Demim]Br|Nafion|HRP|GCE (trace c, Fig. 4(C)) towards H_2O_2 has increased by ~144%, compared to that of the TNT|[Demim]Br|Nafion|HRP|GCE (trace c, Fig. 4(B)), indicating a stronger catalytic effect of HRP in the MWCNT–TNT composite than that in the TNT alone.

The catalytic reduction mechanism of both HRP biosensors in the presence of H_2O_2 can be described by a series of previously reported reactions (Xiao et al., 2000):

$$\mathrm{HRP(Fe^{3+})+H_2O_2 \rightarrow Compound\ I\ (Fe^{4+}=O)+H_2O} \quad (1)$$

$$\mathrm{Compound\ I\ (Fe^{4+}=O)+e^- + H^+ \rightarrow Compound\ II} \quad (2)$$

$$\mathrm{Compound\ II + e^- + H^+ \rightarrow HRP(Fe^{3+})+H_2O} \quad (3)$$

In this scheme, HRP(Fe^{3+}) was firstly oxidised by H_2O_2 to produce Compound I ("$Fe^{4+}=O$" denotes oxyferrite), which could be reduced back to HRP(Fe^{3+}) after successively receiving two electrons from the electrode, as shown in Eqs. (2) and (3). In the absence of H_2O_2, HRP(Fe^{3+}) can be directly reduced to HRP(Fe^{2+}) by gaining one electron from the electrode, as displayed in Eq. (4) below, which accounts for the enhanced reduction current obtained from the same biosensor in the presence of H_2O_2.

$$\mathrm{HRP(Fe^{3+})+e^- \rightarrow HRP(Fe^{2+})} \quad (4)$$

3.5. *Analytical performance comparison between MWCNT–TNT composite and TNT modified HRP biosensors*

As demonstrated in Section 3.3, HRP has shown strong catalytic reduction capability towards H_2O_2 at both MWCNT–TNT composite and TNT modified biosensors. Herein, differential pulse voltammetry was employed to investigate the analytical performances of the HRP biosensors. Fig. 5(A) shows the response of the TNT|[Demim]Br|Nafion|HRP|GCE to the increasing concentrations of H_2O_2 and the inset displays the calibration plot constructed based on the differential pulse voltammetric response subtracting reduction current of HRP (trace a) *versus* H_2O_2 concentrations. As expected, the voltammetric response increased with increasing H_2O_2 concentration from 0.0 to 1.0 mM. For the TNT|[Demim]Br|Nafion|HRP biosensor, the calibration plot can be represented by the relationship,

$$\mathrm{Peak\ current/\mu A = 1.15 \pm 0.024 + 1.48 \pm 0.055/\mu A\ mM^{-1}\ [H_2O_2]}$$

with a correlation coefficient of 0.991 (which was determined to be statistically significant at the 95% confidence level by Student's *t* test; $N=6$). Using the slope of the calibration plot as an estimate, the sensitivity of the TNT|[Demim]Br|Nafion|HRP biosensor is evaluated to be 1.48 μA mM^{-1}. The TNT|[Demim]Br|Nafion|HRP biosensor also displayed a linear range between 0.04 and 1.0 mM.

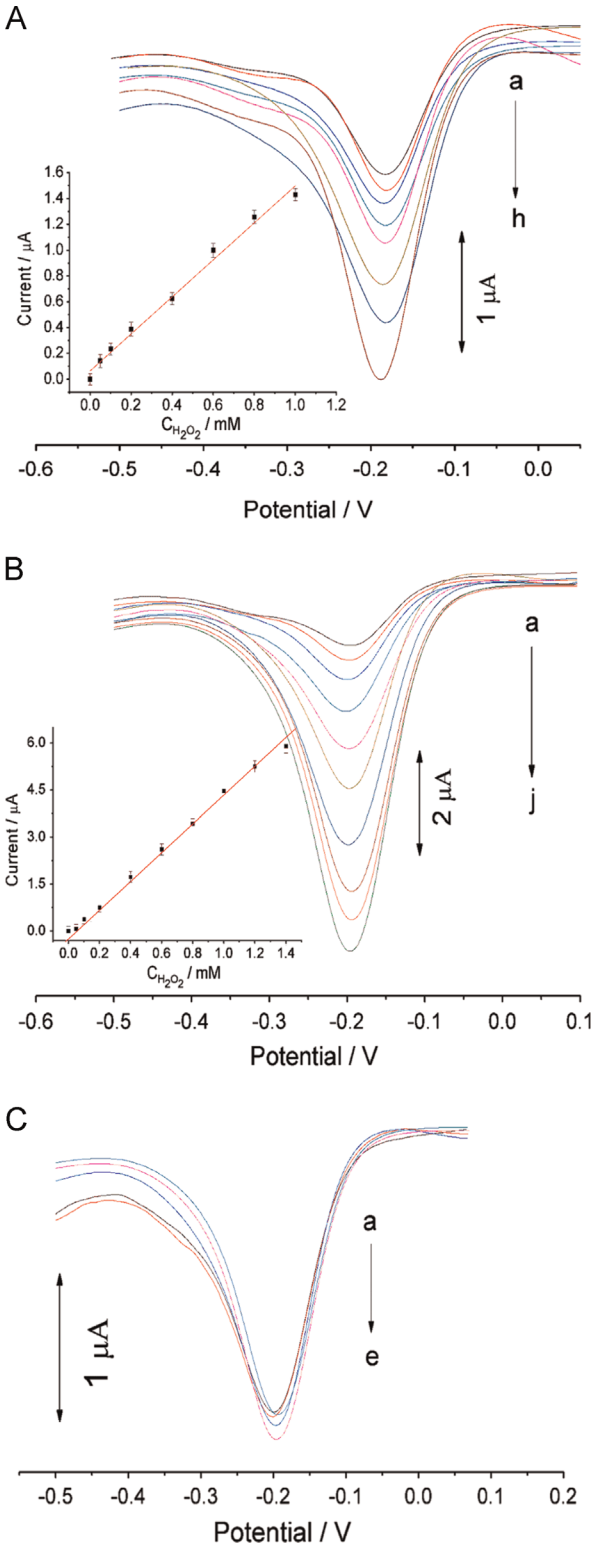

Fig. 5. (A) Differential pulse voltammograms of 50 mM N_2-saturated PBS (pH 7.2) containing (a) 0.0, (b) 0.05, (c) 0.1, (d) 0.2, (e) 0.4, (f) 0.6, (g) 0.8 and (h) 1.0 mM H_2O_2 at a TNT|[Demim]Br|Nafion|HRP|GCE. The inset shows the linear relationship between the catalytic reduction peak current and H_2O_2 concentration; (B) Differential pulse voltammograms of 50 mM N_2-saturated PBS (pH 7.2) containing (a) 0.0, (b) 0.05, (c) 0.1, (d) 0.2, (e) 0.4, (f) 0.6, (g) 0.8, (h) 1.0, (i) 1.2 and (j) 1.4 mM H_2O_2 at a MWCNT–TNT.|[Demim]Br|Nafion|HRP|GCE. The inset shows the linear relationship between the catalytic reduction peak current and H_2O_2 concentration; (C) Differential pulse voltammograms of 50 mM N_2-saturated PBS (pH 7.2) containing (a) 0.2 mM H_2O_2, (b) 0.2 mM H_2O_2 and 0.2 mM ascorbic acid, (c) 0.2 mM H_2O_2 and 0.2 mM dopamine, (d) 0.2 mM H_2O_2 and 0.2 mM cysteine, (e) 0.2 mM H_2O_2 and 0.2 mM uric acid at a MWCNT–TNT.|[Demim]Br|Nafion|HRP|GCE.

Table 1
Analytical performance of several H_2O_2 biosensors.

HRP biosensors	Linear Range/μM	Sensitivity/μA mM^{-1}	Limit of detection/μM	References
(1) Nafion|HRP-GNS[a]-TiO_2|GCE	41–630	0.23	5.9	(Wang et al., 2010)
(2) HRP|RTIL[b]|GNP[c]-TNT|Nafion|GCE	5–1000	0.81	2.1	(Liu et al., 2012)
(3) HRP|HNT[d]|Chi[e]|GCE	2.6–75	12	0.7	(Sun et al., 2010)
(4) Nafion|HRP|Zr-IP_6[f]|GCE	0.67–6	7.8	0.53	(Dong et al., 2010)
(5) Ti/TiO_2/Au/HRP biosensor	5–400	Not reported	2	(Kafi et al., 2008)
(6) MWNTs/chitosan coated GCE	16.7–740	4.9	10.3	(Qian and Yang, 2006)
MWCNT–TNT|[Demim]Br|Nafion|HRP	30–1400	4.4	1.1	This work

[a] Gold nano-seeds.
[b] Room temperature ionic liquid.
[c] Gold nanoparticles.
[d] Halloysite nanotubes.
[e] Chitosan.
[f] Zirconium phytate film.

Fig. 5(B) shows the differential pulse voltammetric response of the MWCNT–TNT|[Demim]Br|Nafion|HRP|GCE in detecting various concentrations of H_2O_2 and the calibration plot is presented in the inset of Fig. 5(B). The calibration plot obtained at the MWCNT–TNT|[Demim]Br|Nafion|HRP|GCE can be represented by the linear relationship,

$$\text{Peak current}/\mu A = 1.23 \pm 0.033 + 4.42 \pm 0.095/\mu A\ mM^{-1}\ [H_2O_2]$$

with a statistically significant correlation coefficient of 0.996 at the 95% confidence level; ($N=6$). Accordingly, a sensitivity of 4.42 μA mM^{-1} and a linear range of 0.03 to 1.4 mM were achieved at the MWCNT–TNT|[Demim]Br|Nafion|HRP|GCE. The analysis above clearly showed an enhanced sensitivity and a wider linear range of the MWCNT–TNT composite modified HRP biosensor compared to those of the TNT modified HRP biosensor, which can be attributed to the higher electrical conductivity of MWCNT–TNT nanocomposite than those of TNTs alone.

The analytical performance, in terms of linear range, sensitivity and limit of detection, of the MWCNT–TNT|[Demim]Br|Nafion|HRP|GCE were also compared to those of several other HRP biosensors, as tabulated in Table 1. The linear range and sensitivity of our biosensor are ~3 and ~19 times, respectively, larger than those of biosensor (1), demonstrating the efficiency of TNTs as an immobilisation matrix over TiO_2 nanoparticles. Although biosensor (2) displayed a ~4 times wider linear range than that of our biosensor, its sensitivity is 20% lower, most likely due to low quantity of gold nanoparticles on the TNT surface of biosensor (2). Attributed to the synergistic effect of MWCNT, TNTs and ionic liquid, our biosensor has shown a significantly lower detection limit than those of biosensor (1) and (2). Both biosensor (3) and (4) show ~3 and ~2 times, higher sensitivity, respectively, compared to our biosensor, but the linear range of our biosensor is ~2 and ~5 times correspondingly wider than that of biosensor (3) and (4). In addition, the limit of detection of our biosensor is comparable to those of biosensor (3) and (4). We attributed these analytical characteristics to the higher conductivity but lower biocompatibility of MWCNT–TNT than those of halloysite nanotube-chitosan composites and zirconium phytate films. Our biosensor also displays improved detection limit and linear range than the HRP biosensor (5) that was based on a Au modified TiO_2 nanotube array, which demonstrated better biocompatibility of TNTs than that of TiO_2 nanotube array. Although a MWCNT modified HRP biosensor (6) shows better sensitivity than ours, the high charging current and low signal-to-noise ratio of the carbon material might have negatively affected their linear range and limit detection. All the above results have provided supporting evidence for the advantages of a biosensor scaffold consisting of titanate–carbon nanocomposites over that composed of only single components. Overall, our biosensor shows superb analytical characteristics over the others considering the balance of linear range, sensitivity and limit of detection.

3.6. Stability, precision and interference test of the biosensor

The stability, precision and interference of MWCNT–TNT|[Demim]Br|Nafion|HRP|GCE were studied using differential pulse voltammetry. In the stability test, based on the mean of triplicate measurements obtained at four biosensors, the response to 0.2 mM H_2O_2 was found to diminish by only 3%, 7% and 13% after being stored at 4 °C for one week, two weeks and four weeks, respectively, indicating the good stability of MWCNT–TNT|[Demim]Br|Nafion|HRP|GCE.

The repeatability of the biosensor was evaluated by 8 successive measurements at a H_2O_2 concentration of 0.2 mM and a relative standard deviation of 1.5% was obtained. In addition, reproducibility was studied based on the detection signals of six biosensors (fabricated in same batch) to 0.2 mM H_2O_2. A relative standard deviation of 5.9% was obtained, indicating an acceptable degree of fabrication reproducibility of the biosensors.

The interferences to the biosensors were evaluated by determination of 0.2 mM H_2O_2 in the presence of several possible coexisting interferences in PBS including ascorbic acid, dopamine, uric acid and cysteine at the same concentration as H_2O_2. In general, interfering species are not expected to be present at a level higher than that of analytes. Here, we have deliberately set all interfering species at the same concentration as H_2O_2 to represent the maximum possible levels to study their effects. As shown Fig. 5 (C), the amperometric response varied less than 8.5%, after spiking 0.2 mM interferences listed above, respectively, into 0.2 mM H_2O_2 solution, which demonstrated high selectivity and strong anti-interference ability of the MWCNT–TNT|[Demim]Br|Nafion|HRP|GCE.

4. Conclusion

In the present work, a MWCNT–TNT nanocomposite has been synthesised and characterised by TEM, XRD, FT-IR and electrochemical impedance spectroscopy. HRP biosensors based on MWCNT–TNT nanocomposite, TNTs alone and MWCNTs alone were constructed and their electrochemical and analytical behaviour was studied using cyclic voltammetry and differential pulse voltammetry. As an electrode immobilisation material, the MWCNT–TNT nanocomposite demonstrated a low background charging current, a high signal-to-noise ratio and small electrochemical interference from the surface functional groups, which is contrast to the performance of MWCNT modified electrode. The

biosensors based on the MWCNT–TNT nanocomposite also showed superiority over those based on TNTs in the electrocatalytic capability and analytical performance, attributable to the high electrical conductivity of MWCNTs. In summary, the MWCNT–TNT nanocomposite has reached a balance between electrical conductivity and biocompatibility and has shown promising properties in constructing practical electrochemical biosensors.

Acknowledgments

This work was financially supported by the China Postdoctoral Science Foundation (No. 2012M511569), the Key Research Project of Henan Educational Department (No. 13A150090) and the Scientific Research Foundation for the Returned Overseas Chinese Scholars, State Education Ministry (Batch 46th).

References

Chen, H., Yang, S., Yu, K., Ju, Y., Sun, C., 2011. J. Phys. Chem. A 115, 3034–3041.
Coleman, J.N., Khan, U., Blau, W.J., Gunko, Y.K., 2006. Carbon 44, 1624–1652.
Dong, J., Wen, Y., Miao, Y., Xie, Z., Zhang, Z., Yang, H., 2010. Sens. Actuators B: Chem. 150, 141–147.
Holland, J.T., Lau, C., Brozik, S., Atanassov, P., Banta, S., 2011. J. Am. Chem. Soc. 133, 19262–19265.
Iwabuchi, A., Choo, C.-k., Tanaka, K., 2004. J. Phys. Chem. B 108, 10863–10871.
Joo, J., Kwon, S.G., Yu, T., Cho, M., Lee, J., Yoon, J., Hyeon, T., 2005. J. Phys. Chem. B 109, 15297–15302.
Kafi, A.K.M., Wu, G., Chen, A., 2008. Biosens. Bioelectron. 24, 566–571.
Lin, Y., Wu, G.S., Yuan, X.Y., Xie, T., Zhang, L.D., 2003. J. Phys.: Condens. Matter 15, 2917.
Liu, X., Feng, H., Zhao, R., Wang, Y., Liu, X., 2012. Biosens. Bioelectron. 31, 101–104.
Liu, X., Zhang, J., Liu, S., Zhang, Q., Liu, X., Wong, D.K.Y., 2013. Anal. Chem. 85, 4350–4356.
Muduli, S., Lee, W., Dhas, V., Mujawar, S., Dubey, M., Vijayamohanan, K., Han, S.-H., Ogale, S., 2009. ACS Appl. Mater. Interfaces 1, 2030–2035.
Pang, X., He, D., Luo, S., Cai, Q., 2009. Sens. Actuators B: Chem. 137, 134–138.
Perera, S.D., Mariano, R.G., Vu, K., Nour, N., Seitz, O., Chabal, Y., Balkus, K.J., 2012. ACS Catal. 2, 949–956.
Pizem, H., Sukenik, C.N., Sampathkumaran, U., McIlwain, A.K., De Guire, M.R., 2002. Chem. Mater. 14, 2476–2485.
Pumera, M., Sánchez, S., Ichinose, I., Tang, J., 2007. Sens. Actuators B: Chem. 123, 1195–1205.
Qian, L., Yang, X., 2006. Talanta 68, 721–727.
Qureshi, A., Kang, W.P., Davidson, J.L., Gurbuz, Y., 2009. Diam. Relat. Mater. 18, 1401–1420.
Serafín, V., Hernández, P., Agüí, L., Yáñez-Sedeño, P., Pingarrón, J.M., 2013. Electrochim. Acta 97, 175–183.
Si, P., Ding, S.J., Yuan, J., Lou, X.W., Kim, D.-H., 2011. ACS Nano 5, 7617–7626.
Sun, X., Zhang, Y., Shen, H., Jia, N., 2010. Electrochim. Acta 56, 700–705.
Suzuki, Y., Yoshikawa, S., 2004. J. Mater. Res. 19, 982–985.
Wang, H., Wang, H.-L., Jiang, W.-F., Li, Z.-Q., 2009a. Water Res. 43, 204–210.
Wang, J., Tafen, D.N., Lewis, J.P., Hong, Z., Manivannan, A., Zhi, M., Li, M., Wu, N., 2009b. J. Am. Chem. Soc. 131, 12290–12297.
Wang, S., Zhou, S., 2011. J. Hazard. Mater. 185, 77–85.
Wang, Y., Ma, X., Wen, Y., Xing, Y., Zhang, Z., Yang, H., 2010. Biosens. Bioelectron. 25, 2442–2446.
Xiao, Y., Ju, H.-X., Chen, H.-Y., 2000. Anal. Biochem. 278, 22–28.
Yang, J., Jin, Z., Wang, X., Li, W., Zhang, J., Zhang, S., Guo, X., Zhang, Z., 2003. Dalton Trans., 3898–3901.
Zhang, M., Jin, Z., Zhang, J., Guo, X., Yang, J., Li, W., Wang, X., Zhang, Z., 2004. J. Mol. Catal. A: Chem. 217, 203–210.
Zhang, Z., Xie, Y., Liu, Z., Rong, F., Wang, Y., Fu, D., 2011. J. Electroanal. Chem. 650, 241–247.